Journal of Fusion Energy (2023)42:4
https://doi.org/10.1007/s10894-023-00342-2

REVIEW ARTICLE

The Princeton Field-Reversed Configuration for Compact Nuclear Fusion Power Plants

Christopher Galea[1] · Stephanie Thomas[1] · Michael Paluszek[1] · Samuel Cohen[2]

Accepted: 15 January 2023

Abstract

The Princeton Field-Reversed Configuration (PFRC) nuclear fusion reactor concept is an innovative approach to fusion power generation prioritizing low neutron production and small size. A combination of analytical modeling and numerical simulation shows that the novel heating approach generates an FRC with closed field lines. Simulation data from a single-particle Hamiltonian code predicts ms-scale plasma heating in reactor-scale conditions while PIC codes predict formation of warm FRC plasmas from initial mirror fields. The PFRC-1 and PFRC-2 experiments have heated electrons to energies well in excess of 100 eV and plasma durations to 300 ms, more than 10^4 times longer than the predicted tilt instability growth time. From these data, we have created a development plan and anticipated performance metrics for a fusion reactor based on the PFRC concept. The resulting 1–10 MW PFRC reactors would be suitable for diverse applications, from submarines to urban environments to space propulsion. PFRC is a steady-state, driven magnetic confinement device. Plasma, inside a cylindrical array of coils, is confined and heated by external RF antennae. PFRC would be ultra-low radiation due to both its fuel and small size. The choice of advanced fuels, deuterium and helium-3 (D–^{3}He), may be enabled by the high-β FRC configuration. The small size of the reactor would enable rapid exhaust of the dangerous tritium ash. Low radiation would make the reactor safer to operate and, in combination with simple geometry and small size, dramatically lowers development and maintenance costs. This review paper gives an introduction to the physics of the PFRC and a summary of the PFRC-2 experiment results to date. It then discusses the future program plan and how PFRC reactors would be commercialized.

Keywords Nuclear fusion · Field-reversed configuration · Magnetic confinement fusion · Modular power · Space propulsion

Christopher Galea, Stephanie Thomas, MichaelPaluszek and Samuel Cohen contributed equally to this work.

✉ Christopher Galea
cgalea@princetonfusionsystems.com

Stephanie Thomas
sjthomas@princetonfusionsystems.com

Michael Paluszek
map@princetonfusionsystems.com

Samuel Cohen
scohen@pppl.gov

[1] Princeton Fusion Systems, 6 Market Street, Suite 926, Plainsboro, New Jersey 08536, USA

[2] Program in Plasma Science and Technology, Princeton Plasma Physics Laboratory, 100 Stellarator Road, Princeton, New Jersey 08540, USA

Published online: 31 January 2023

Introduction

Nuclear fusion is a potential source of power for a wide variety of applications, ranging from power for the grid to deep space propulsion. Numerous fusion projects are underway, supported by both private firms and government entities. Tokamaks are the major type of machine under development, notably by ITER, Tokamak Energy, and Commonwealth Fusion Systems. Other magnetic confinement schemes include mirrors, operating at the University of Maryland and University of Wisconsin, Stellarators at the Max-Planck Institute, and FRCs at the Princeton Plasma Physics Laboratory (PPPL), TAE Technologies, and Helion Energy. TAE is pursuing p–^{11}B fusion while Helion is pursuing D–^{3}He and D–D fusion.

The Princeton Field-Reversed Configuration (PFRC) is a novel reactor class. As described later, it would use only one RF system, odd-parity Rotating Magnetic Field (RMF$_o$), to drive plasma current, heat the plasma, improve confinement, and provide stability. PFRCs would burn deuterium and helium-3, (D–^{3}He), a fuel mixture that generates little radioactivity. The relatively small machine would promote rapid exhaust of the tritium (T) produced by D-D side reactions, [1, 2] further reducing the neutron wall load. Electricity would be produced using a Brayton cycle with a helium/xenon working fluid and thermalization of X-ray and synchrotron radiation emitted from the plasma. The machine is intended for compact, mobile, and modular applications, including space propulsion. [3–6] For military forward power, a 1-MW PFRC could be mounted on an HEMTT truck, as shown in Fig. 1.

Prior work for forming FRC plasmas with RMF have typically used a picture-frame antenna that resulted in a near-FRC plasma but with open magnetic field lines. We call this even-parity heating, RMF$_e$, due to the symmetry of the induced magnetic field. [7–9] RMF$_e$ was proposed to drive current in the plasma, not to heat it to fusion temperatures. However, RMF$_e$ produces open field lines that allow the plasma to escape, hence reducing energy confinement time. RMF$_o$, first theorized in 2000, was predicted to maintain an FRC's closed field-line structure and heat ions to fusion-relevant temperatures. [10, 11] The original prediction of closed field lines used a graphical method and has been recently reproduced by an analytical model. [12] FRC formation by RMF$_o$ has been modeled using particle-in-cell (PIC) simulations. [13] In the case of RMF$_o$, each of the four RF antenna sections are two joined rectangles, not a single picture-frame. In this antenna configuration the magnetic field on one side of the plasma's axial midplane is in the opposite direction as the other side, producing a first-order current drive because of an O-point magnetic null line near the FRC's midplane. The azimuthal RMF$_o$-generated electric field near that null directly accelerates charged particles into betatron orbits, ions in one direction and electrons in the opposite.

Fig. 1 Truck mounted 1 MWe PFRC.

Electron energization results from the same azimuthal acceleration created by the RMF$_o$-induced electric field. Axial electron acceleration is also caused by RMF$_o$-induced electric fields. The necessary loss-of-phase for net electron heating to be generated by the RMF is caused by both Speiser collisions with the magnetic field's changing curvature and passage near the field nulls. The ion heating mechanism may be viewed differently, by the ions moving in near synchronization with the RMF$_o$. Explosive ion heating to D–^{3}He-fusion temperatures has been predicted by the RMF code, [11, 14–16] see Fig. 2. Initial benchmarking of the RMF code has been conducted in the first iteration of PFRC, the PFRC-1 device, where the measured average electron energies agreed well with code predictions. [17] Stabilization against interchange modes has been seen in several RMF-FRC experiments. The explanations vary: the ponderomotive force; dynamic stabilization; and other RF effects. [18]

The PFRC-2 is an experiment currently operating at the Princeton Plasma Physics Laboratory. [19–21] The growth rate of the tilt mode, $\sim 1/\tau_t$, is estimated, in a fluid model, to be the ion sound speed divided by the machine length. τ_t is near 1 μs in the PFRC-2. Contradicting the fluid-based theory, PFRC-2 discharges of 300-ms duration have been sustained. The near-term PFRC-2 research plan is to raise the axial magnetic field to over 1 kG, lower the RMF frequency to 2 MHz, and increase the RMF field strength to 15 G. At these levels, theory predicts entry into the ion heating regime.

In the next-step PFRC device, PFRC-3, studies will be made of RMF$_o$ antenna configurations, reduction of heat loss across the separatrix, and operation at higher plasma pressure, all in hydrogen plasmas. A reactor prototype PFRC, PFRC-4, would then be built with a goal of producing more than 100 kW of quasi-steady-state fusion power. The reactor prototype, using D-^{3}He, would be used

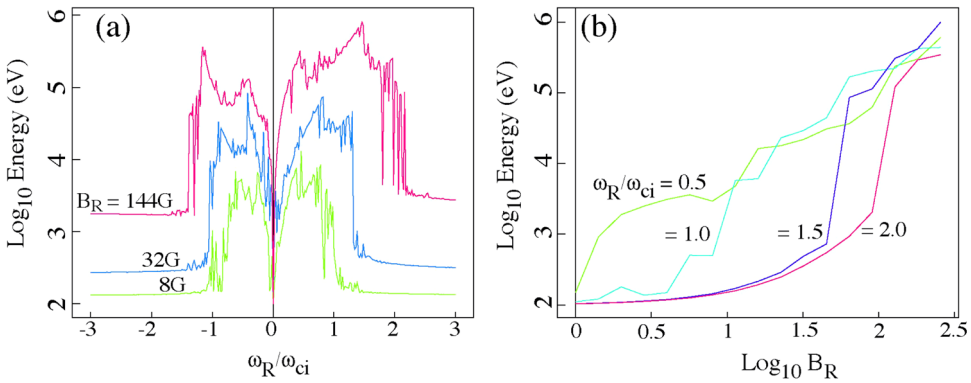

Fig. 2 Ion heating as predicted by the RMF code. [11, 14–16] The reference FRC parameters are radius of 10 cm, elongation of 5, and center-plane axial field (central field) of 20 kG. B_R is the strength of the RMF field and ω_R/ω_{ci} is the ratio of the RMF frequency to the ion cyclotron frequency at the central field.

to study the T-ash extraction method envisioned to be possible only in PFRC-type reactors.

Overview of the PFRC Reactor Concept

The PFRC employs a unique radio frequency (RF) plasma heating method, RMF$_o$. When scaled up to achieve fusion parameters, PFRC-type power-producing reactors would be 4-8 m long and 1.5 m diameter and produce 1 to 10 MW of fusion power. By methods to be soon described, PFRC reactors would be uniquely small and clean among all fusion reactor concepts, producing very low levels of damaging neutrons. This greatly reduces the need for materials development, reactor maintenance, and siting restrictions.

PFRC Concept of Operations

A diagram of the fusion reactor is shown in Fig. 4. Fusion fuel is injected into the reactor core with relatively low power neutral beams operating at 10's of kV. [22] Note the active trim coils for plasma shape control.

Additional power plant subsystems are shown in Fig. 3. The startup system, for energizing the coils and starting the fusion reaction, is shown as a diesel generator. [23] Other startup methods are under consideration. The fusion vacuum vessel is shown in orange. The RMF generator system is depicted above the vacuum vessel. Coil refrigeration is on the right. The heat recycling system – i.e., a Brayton cycle thermal conversion system, [24] – is on the bottom.

As in D-T tokamak reactors, where 85% of the fusion power is not deposited in the plasma but leaves with the neutrons, little fusion power is deposited in the PFRC core by its fusion products. Because of the PFRC's relatively small size, the charged fusion-product orbits extend outside the separatrix and pass through cold plasma there, termed the energy and ash removal shell. The shell rapidly extracts the energy from the fusion products, *ca.* 10 ms, and also removes the ash, avoiding the harmful ash build-up of such concern in tokamaks. This unique ash removal feature, enabled by the small size of the FRC, is a key improvement from previous D–^{3}He FRC reactor concepts. [25–28] The cold shell plasma is sourced by deuterium gas injected in the source chamber, see Fig. 4. The heat engine collects the energy from radiation losses to the reactor walls and from the exhaust box end wall. X rays would be thermalized with tungsten films or foil. A high-efficiency recuperated Brayton cycle would generate electricity, a fraction of which is used to drive the RMF$_o$. Excess heat is released to the environment. The deuterium in the cool shell plasma and fusion products are separated from each other, first in the exhaust chamber and with further processing down stream.

PFRC has a high Carnot efficiency because the working fluid cooling the reactor can reach up to 1500 K with ceramic heat-exchanger materials. High-temperature gas-cooled fission reactors can also reach high efficiencies, but water-cooled cannot. As noted earlier, D-T machines release most of their energy as neutrons whose energy is absorbed by a lithium blanket. The peak temperature is limited by the blanket properties.

RMF$_o$ Heating Method

The RMF$_o$ plasma heating method uses a unique configuration of the radio frequency antenna. In the present experiment, each of the four PFRC antenna sections are two joined rectangles. Two pairs operate 90° out-of-phase on adjacent sides of the plasma. An antenna (wrapped in orange Kapton tape) is visible on the side of PFRC-2 in Fig. 5.

This antenna configuration produces an odd-parity magnetic field — the magnetic field on one side of the plasma's axial midplane is in the opposite direction as the other side. The phase of the current oscillations in the RF antenna results in a rotating magnetic field, RMF, of strength 0.1-5% of that of the axial magnetic field. As noted before, odd-parity RMF maintains an FRC's closed field lines. [10, 12] Closed field lines keep the plasma and

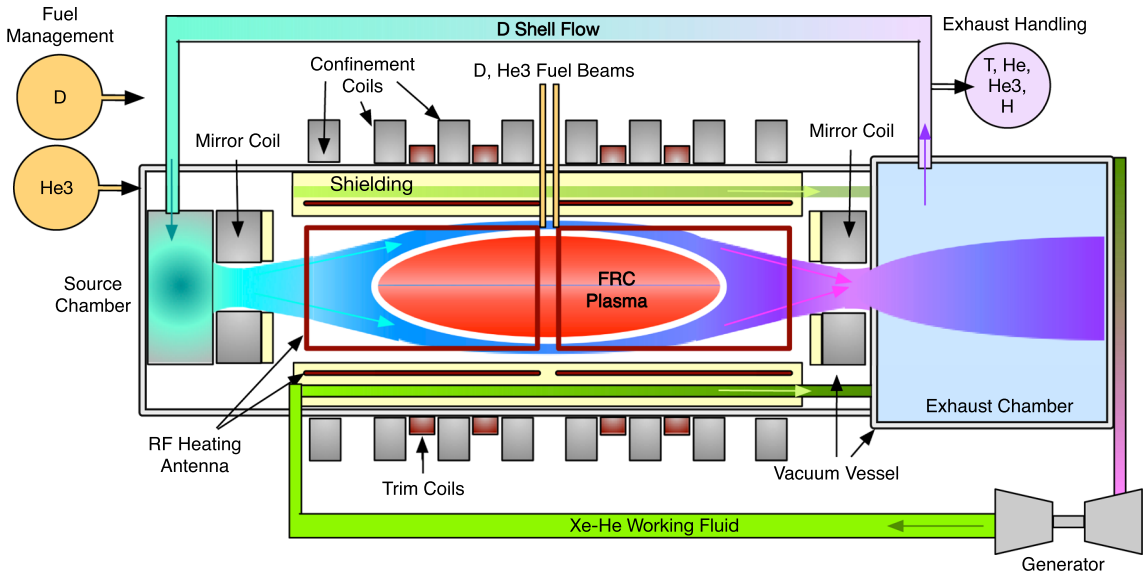

Fig. 3 Schematic of the PFRC reactor concept. The antenna and shielding geometry are notional.

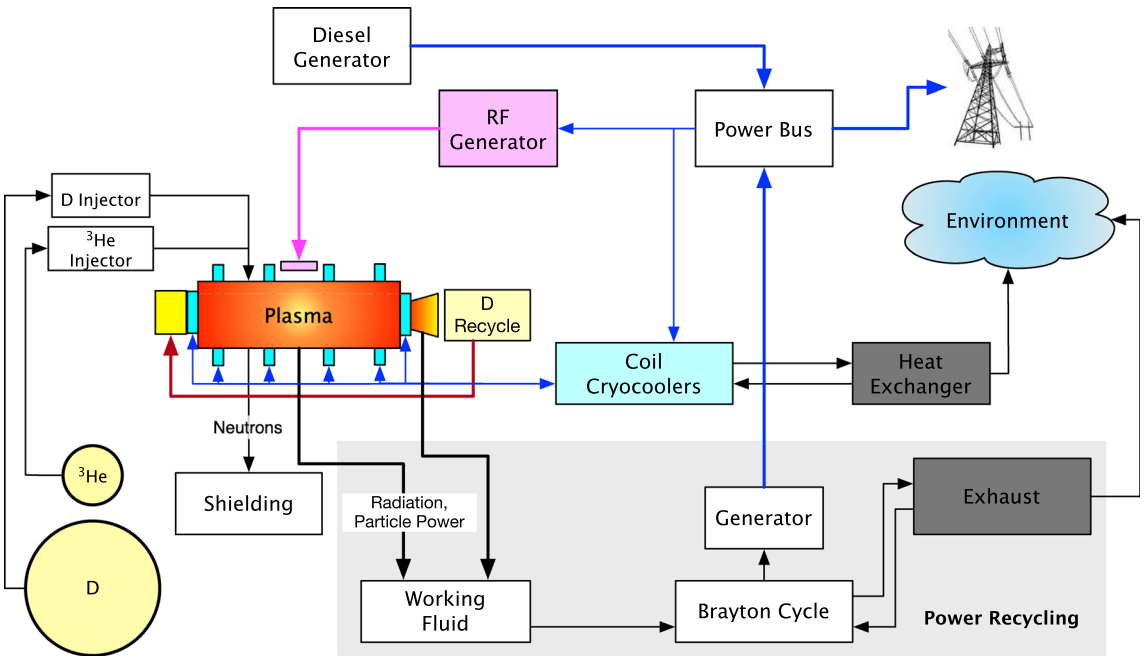

Fig. 4 PFRC block diagram with additional power plant subsystems.

its energy trapped as the plasma is heated. Fig. 6 shows a Grad-Shafranov solution of the closed field lines in the PFRC.

Ideally, for simplest design and operation, the RMF antennae would be located outside the vacuum vessel and shielding, as they are on PFRC-2. However, this requires all inboard components to be non-conductive and the additional distance may impact RF penetration. Therefore, the antenna may need to be embedded somewhere within the shielding structure. This may introduce paths for neutron scattering up the power flow channel. One prospective antenna shielding material is Boron-10, which has a high neutron absorption cross-section and low conductivity, although the conductivity rises significantly at higher temperatures. This presents a trade-off between neutron shielding and RMF penetration dependent on the antenna distance from the plasma and the location of the heat exchangers. The optimal design and placement of the RMF$_o$ antennas will be investigated under an ongoing DOE INFUSE grant.

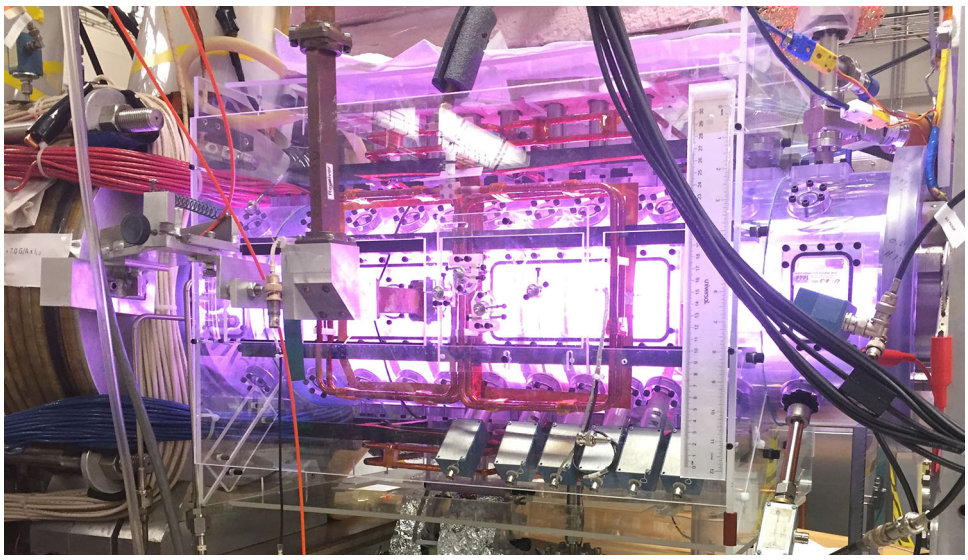

Fig. 5 A plasma shot in the PFRC-2 experiment at PPPL.

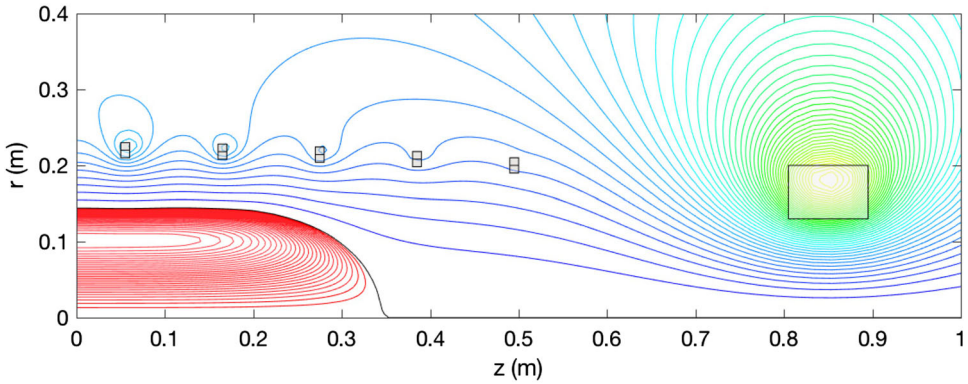

Fig. 6 Closed field lines as predicted in the PFRC core by a Grad-Shafranov code. The cool shell plasma will flow along the open field-lines to extract the fusion energy and ash. [29]

Power Flow and Neutron Loads

We have studied the power flow throughout the PFRC-reactor system using a 1D FRC model that assumes a Hill's vortex density scaling and uniform temperature. Fig. 7 shows the power flow model for a 2 MWt reactor with 0.79 MW of RMF power and assuming a 50% efficient Brayton cycle. The RMF power is produced with efficiency greater than 90% using class D or E amplifiers. The net electric power generated is 0.57 MW. Compared to the figure in

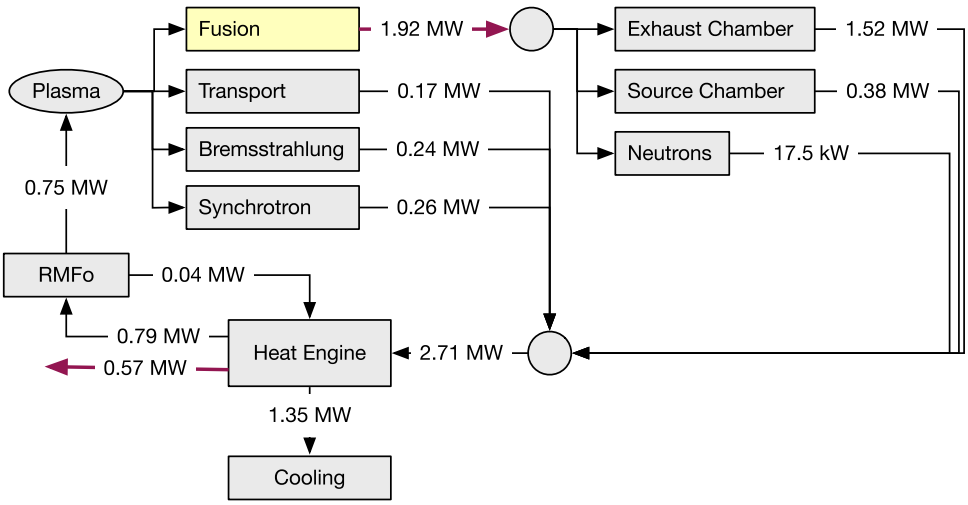

Fig. 7 Power flow model using 1-D PFRC reactor scaling. The "gas box" is the source chamber. This assumes a plasma radius of 25 cm and elongation of 3, fuel ratio of 1:1, ion temperature of 100 keV, central field of 5.5 T, and 98% wall reflection of synchrotron with classical confinement. [34] The resulting equilibrium electron density and temperature is 5.7×10^{20} m^{-3} and 66 keV.

[29], this diagram includes transport losses. Particle-in-cell models are allowing studies, now in progress, of methods to maintain or improve the energy confinement. Scaling to a reactor requires an energy confinement near classical. TAE FRCs have achieved that quality at the keV ion-temperature level. [30–33]

The PFRC is specifically designed to have low neutron level, about 1000 times lower wall loading, *i.e.,* neutron power flux (W/m^2) on the inner wall, than D-T tokamaks. Being high-β machines, where β is the ratio of the plasma pressure to the magnetic-field energy density, FRCs should achieve the high temperatures necessary to burn the advanced fuel mixture, ^{3}He and D, at a relatively low magnetic field. D-^{3}He fusion requires achieving ~ 100 keV ion temperatures. The D-^{3}He fusion reaction results in no damaging neutrons. Low-energy neutrons would be created by the low level of D-D fusion reactions; high energy neutrons would be created if the T fusion product was not extracted quickly. The rapid extraction of T is one reason for the shell plasma. The reaction equations are:

$$\mathrm{D} + {}^3\mathrm{He} \rightarrow {}^4He\ (3.6\ \mathrm{MeV}) + \mathrm{p}\ (14.7\ \mathrm{MeV}) \quad (1)$$

$$\mathrm{D} + \mathrm{D} \rightarrow \mathrm{T}\ (1.01\ \mathrm{MeV}) + \mathrm{p}\ (3.02\ \mathrm{MeV}) \quad (2)$$

$$\mathrm{D} + \mathrm{D} \rightarrow {}^3\mathrm{He}\ (0.82\ \mathrm{MeV}) + \mathrm{n}\ (2.45\ \mathrm{MeV}) \quad (3)$$

$$\mathrm{D} + \mathrm{T} \rightarrow {}^4\mathrm{He}\ (3.5\ \mathrm{MeV}) + \mathrm{n}\ (14.1\ \mathrm{MeV}) \quad (4)$$

Burning D–^{3}He at high temperatures in a tokamak or large FRC reactor could result in an increase in neutrons due to the above reactions, a five times higher heat load on the divertor plates than the currently predicted heat loads in tokamaks, and consumption of the world's ^{3}He supply in a few weeks.

A PFRC-type reactor has three design features to greatly reduce the number and impact of the neutrons from this baseline: 1) the small size of the reactor (~ 25 cm plasma radius) results in a favorable ratio of surface area to plasma volume, reducing the wall load compared to larger machines; 2) the fuel-mix ratio of ^{3}He:D can be adjusted upwards to as much as 3:1, sacrificing some power density for lower neutron production; and 3) via the shell, PFRCs are designed to rapidly eliminate the T produced by the D-D side reactions, preventing any D-T reactions from occurring. The only neutrons produced would have an energy of 2.45 MeV. An an example, for 1:1 fuel ratio at 100 keV and electron density of 6×10^{20} per m^3, the rate of D-D neutrons produced is 4.8×10^{17} per m^3 per second. At 30 cm radius, the approximate location of the first wall, the flux is 9×10^{17} n/m^2 (13 kW/m^2).

The T would be eliminated rapidly due to its interaction with the shell surrounding the fusion region. The size of the reactor is characterized by the so-called FRC *s*-parameter, [35] which scales with the ratio of the ion gyro-radius (at the FRC's central field) to the separatrix radius at the midplane. For T fusion products s is low - about 2.5. At such a value, the T fusion products pass through the shell repeatedly. When the T pass through the cool shell plasma, electron drag causes energy to be transferred from the T to the shell electrons. The T is quickly captured by the shell field lines and flows out the open end of the reactor. The burn-up time for energetic T to fuse is about 20 seconds, while classical slowing down theory and particle-in-cell simulations have both shown that the time in which the T will cool and be trapped in the shell is less than 0.01 seconds. [1, 2] Based on this, less than 1% of the T would fuse with the D before it was extracted. The same energy extraction occurs for the other fusion ash products, though at somewhat different rates. By this process all ash is effectively exhausted.

Losses in a Small FRC Reactor

Preliminary loss estimates indicate that a closed reactor design is possible, as indicated in Fig. 7.

A rudimentary estimate of heat conduction loss can be performed based on classical thermal conductivity. We approximate the radial heat flux as $Q_{loss} = k\frac{dT}{dr}A \approx kAT/\Delta r$, where k is the classical transverse thermal conductivity, [36] T is the ion temperature of 100 keV, A is the surface area of the plasma through which the heat flux crosses, and Δr is approximately 1/3 of the plasma radius, since in an FRC the gradient length scale is the difference from the O point field null to the separatrix. Taking the plasma to be a prolate ellipsoid with 25 cm semi-minor axis (plasma radius) and 75 cm semi-major axis (elongation of 3), we estimate $Q_{loss} \sim 0.5$ MW, which is a modest amount compared to the 2 MWt of the reactor. This estimate ultimately has questionable validity as the assumption of small Larmor radius behind Spitzer's formula breaks down near the field null line of an FRC.

For several reasons, PFRCs are expected to have better energy confinement than mainline magnetic confinement fusion devices, hence could be smaller. One, neoclassical transport increases with $(1+q^2)$, where q is the safety factor. In tokamaks stable operation away from the major instability boundaries requires $q > 3$. In FRCs where there is zero toroidal magnetic field and hence only a poloidal magnetic field, $q = 0$. Applying the results of neoclassical theory, FRCs having the same magnetic field and plasma temperature would have 10 times better energy confinement than tokamaks. Results from TAE experiments (as mentioned in the previous subsection) support this. [30–33]

Two, transport in tokamaks is predicted to be enhanced by turbulence because its scale is somewhat larger than the

ion gyro-radius, less than 0.1% of the plasma radius. In a PFRC-type reactor, the orbits of the thermal ions are a considerably larger percentage of the machine size, exceeding 30%. At such a large scale, ion orbits should be far less perturbed by turbulence than in a tokamak.

Three, the plasma in a PFRC will be 10 times hotter than in a D-T tokamak. The effect on confinement of the increased ion gyro-radius will be more than compensated by the decreased collisionality. The net effect will be a 3-fold reduction in the thermal diffusivity. In passing we note that the 10 times higher β in FRCs, compared to tokamaks, balances the higher temperature needed. Hence both operate at the same magnetic field strength, $\sim$6 T.

Status of development: The PFRC-2 Experiment

RMF_o current drive was first demonstrated in the 4-cm plasma radius PFRC-1 experiment in 2006. [17] Experiments are ongoing with the second-generation machine, PFRC-2, which has a flux conserver inner radius of 8 cm (Fig. 5). Results from experimental studies of electron heating in PFRC-2 have surpassed theoretical predictions, with minority electron populations reaching temperatures of 500 eV, maximum energies exceeding 1.5 keV, and pulse lengths up to 300 ms, though typically 10 ms. PFRC-2 has operated with RF frequencies from 4.3 to 12 MHz, forward power up to 100 kW, (central) vacuum magnetic fields of 350 G, and mirror ratios to 30. The coupling efficiency of RF power to the plasma has reached 60%.

PFRC-2 is being upgraded to operate with an RMF frequency of 2 MHz, a compressed magnetic field of up to 0.1 T, and a total RMF forward power of 200 kW. This results in an RMF field strength of up to 15 G. At these parameters, single-particle simulations predict explosive ion heating to energies above 1 keV. [19] Table 1 gives the latest results and the targets for both PFRC-2 and future machine generations. PFRC-4 is envisioned as a prototype reactor power plant with a complete conversion system.

Figure 8 shows examples of the 100- and 250-ms pulses. The line-averaged electron density time traces were measured with a 170-GHz interferometer located $\sim$10 cm from the FRC's midplane. A gas puff of 2 ms duration is shown in the top pulse (green spike).

Figure 9 shows X-ray data measured from a silicon drift detector (SDD). The analysis of X-ray data from PFRC-2 is described in [37]. For this plasma, the SDD X-ray detectors, sensitive to X rays produced by energetic electrons, show bulk electron temperatures of 75 eV. Electron temperatures up to 500 eV have been measured for a minority population of electrons, which, by conservative estimates, comprise about 1% of the bulk density. Recent DEGAS-code Monte-Carlo simulations indicate that the molecular hydrogen density profile in the PFRC-2 core plasma is at least an order of magnitude lower than that at the edges, [38] which would imply higher electron densities from our X-ray analyses, reaching 10% of the bulk density. The X-ray measurements performed were line integrals near the FRC midplane, obtained by viewing the plasma along chords having different tangent radii. The radial profiles measured indicated that the electron energy distribution was relatively constant with respect to radial position.

The next step for PFRC-2 will be the attachment of the Stripping Cell Ion Energy Analyzer [40] that will measure ion temperatures. These experiments are planned for early 2023. Presently we are testing the RMF_o system at the upgraded frequency and preparing to install additional coils that will increase the magnetic field, in order to test the predicted ion heating regime. We have recently been awarded three INFUSE grants which will support computational analyses of different RF antenna configurations and FRC stability, and measurements of electron temperature profiles in the PFRC-2.

The development plan to transition from PFRC-2 to a pilot power plant includes an intermediate PFRC-3 device with a ten times stronger field, about 1 T, [19] to be achieved with a low-temperature superconducting magnet array. PFRC-3 goals include an FRC plasma radius greater than 15 cm, a bulk ion temperature of 10 keV, plasma density of 1×10^{20} m^{-3} and 10 mVs excluded flux, as shown in Table 1.

Commercialization

PFRC reactors would be manufactured in a factory (see Figure 10) and shipped pre-fueled to customers. Current Overnight Capital Cost (OCC) estimates are $8.9M for a 1 MWe reactor and $24.5M for a 10 MWe reactor. This is based on current costs for superconducting magnets and similarly sized gas turbines, specific staff and facility size assumptions, and a production of 20 engines per year. A higher power output is achieved by building a longer PFRC. The magnet costs have a favorable scaling with higher power as the strong mirror magnets are needed regardless of reactor length. The turbine costs scale nearly linearly with the engine power.

PFRC has potential for space, undersea, and surface applications. Uses in space include:

- Robotic spacecraft in the inner and outer solar system including interstellar precursors.
- Power for research and communications.
- Mars base power.
- Lunar base power.

Table 1 PFRC-2 experimental results and PFRC-3 and PFRC-4 targets. [19]

Parameter	PFRC-2 Value	PFRC-3 Goal	PFRC-4 Goal
Pulse length	300 ms	1 s	100 s
Magnetic field strength	to 350 G (vacuum)	1.5 T	6 T
RMF Frequency	2-14 MHz	1 MHz	0.5 MHz
RMF Power	to 200 kW	300 kW	500 kW
RMF Coupling	60%	75%	90%
Plasma temperature		10 keV ions	100 keV ions
Observed	100 eV e^- at 4.3 MHz		
Goal	500 eV ions at 2 MHz		
Plasma radius	8 cm	16 cm	25 cm
Electron density	1×10^{13}/cc	1×10^{14}/cc	6×10^{14}/cc
Fuel	H_2	H_2	D-^{3}He
Excluded flux	0.6 mVs	10 mVs	400 mVs
τ_E (s)	$5x10^{-5}$	0.004	0.4

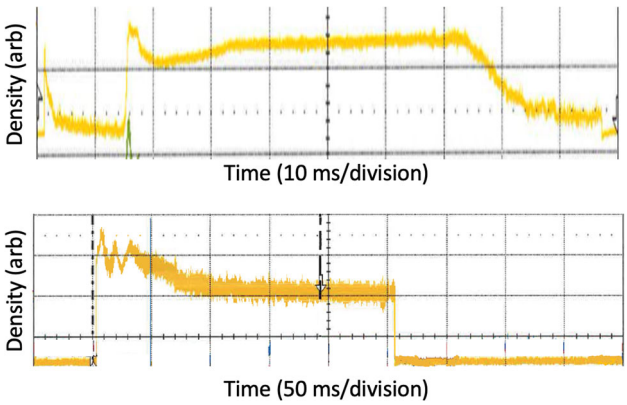

Fig. 8 Density *vs* time for PFRC-2 pulses of 100 ms (top) and 250 ms (bottom) in duration. The top pulse, performed with superconducting internal flux conservers, shows a gas puff (green spike) of 2 ms duration at 15 ms which causes the longer duration of higher plasma density. The time of the gas puff in the bottom pulse is also around 15 ms, which is the trigger for the second and third density spikes.

- Space station power.
- Lunar cargo transporter.
- Human Mars missions.
- Transporting a telescope to the 550 AU point.

A PFRC-powered transfer vehicle could become a standard platform for deep-space and interstellar missions. This was a role NASA envisioned for the Jupiter Icy Moon Orbiter (JIMO) project. [41] JIMO would have carried a nuclear fission reactor that powered electric thrusters and provided electric power to the spacecraft. [42] A PFRC-powered vehicle would dramatically reduce the cost per watt for robotic missions from $14M/watt for NASA's Dragonfly to $2/watt. It can be argued that the scientific return for a robotic mission is proportional to the power as power determines what experiments can operate and how much data can be transmitted. The high available power would enable whole new classes of deep-space scientific instruments.

The U.S. Department of Defense is the largest potential customer for the first production units. The Army wants to move to an all-electric battlefield. [43] The Army has a requirement that its brigades be able to fight for an entire week without resupply. [44] ARPA-E [45] has recognized the need for improved battlefield power supplies and distribution. Defense applications include:

- Forward power for Army brigade combat teams.
- Forward power for Marine expeditionary units.
- Power for small surface combatants and drone submarines [46].
- Power for attack submarines.
- Power to support high-power devices such as rail guns on navel vessels.
- Distributed power for large surface combatants including aircraft carriers.
- Distributed power for ballistic missile submarines.
- Power for laser-armed drones.
- Base power.
- High power satellites (laser, radar, high power communications).

Civilian applications are emergency power, remote power, and power for remote industries. Hurricanes Sandy and Maria showed the need for portable emergency power. In Hurricane Sandy, fossil-fueled vehicles were stranded because fuel pumps were without electric power. Generators were idle due to damage to natural gas lines. Puerto Rico is still suffering the after-effects of Hurricane Maria. Specific civilian application examples are:

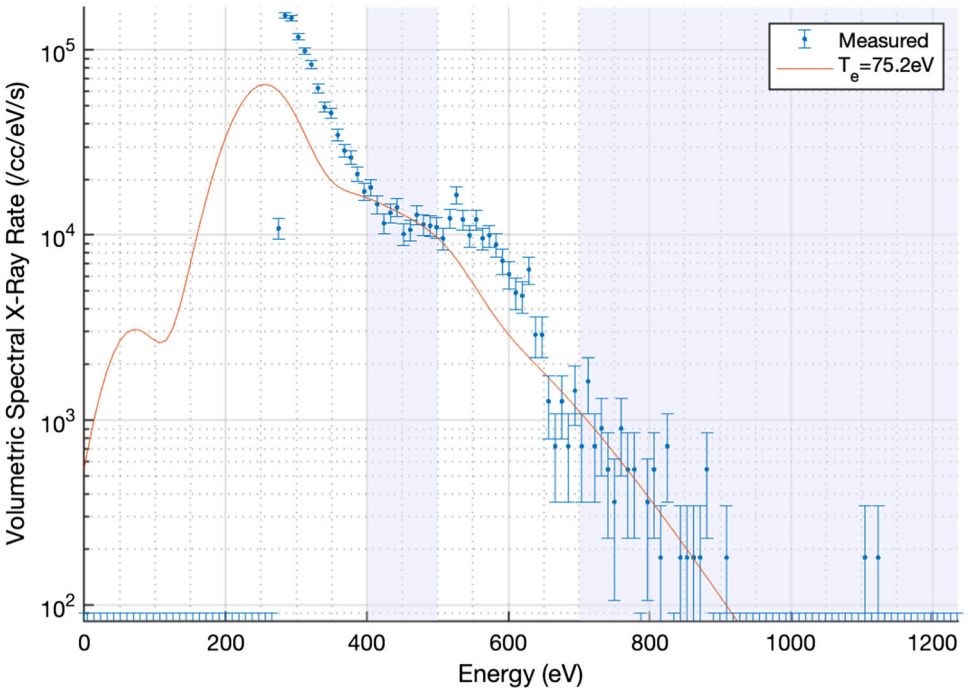

Fig. 9 SDD X-ray data and corresponding Maxwellian fit of 75 eV at an RMF_o frequency of ω_{RMF} = 4.3 MHz and power of 70 kW. [39] The shaded regions show the domain where the fit was applied, where there are no X-ray spectral lines. Corrected for pressure drop during the pulse, the Maxwellian fit density is found to be 6.4×10^{11}/cc, close to the interferometer-measured bulk density of $\sim10^{12}$/cc.

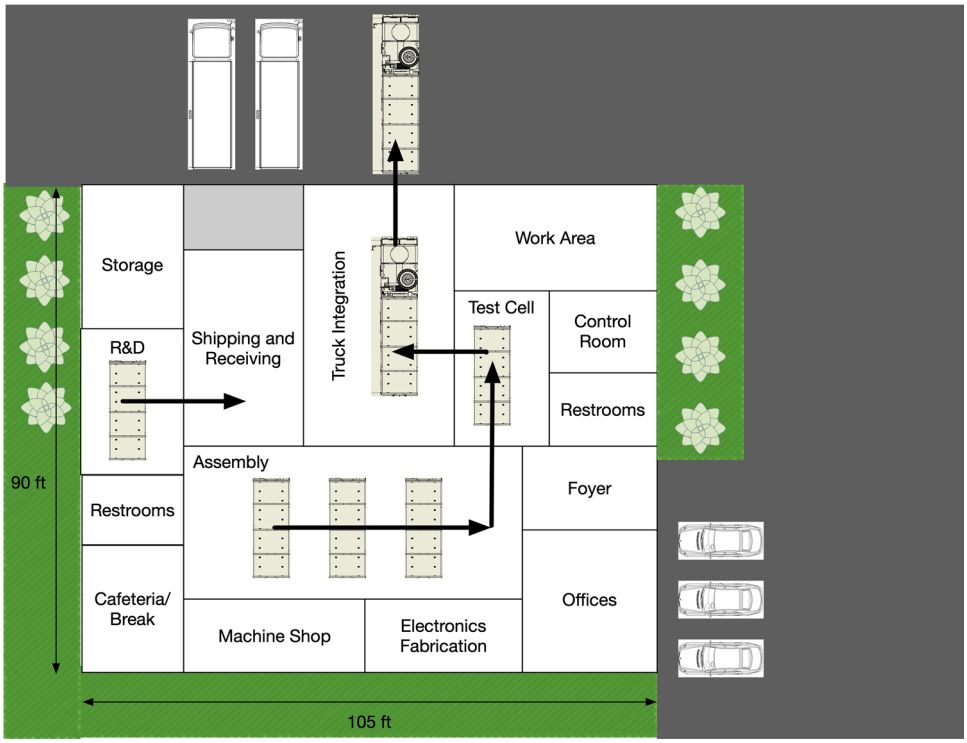

Fig. 10 An assembly plant capable of building twenty 1 MWe PFRCs per year. 1-MWe machines would be the first products.

- Remote towns in Alaska and other regions with poor connection to the power grid. Power can cost up to $1.60/kWh when diesel is delivered by light aircraft. [47]
- Mobile emergency power.
- Power for mines. [48]
- Power for offshore drilling rigs.
- Power for tar sands oil recovery.
- Desalinization power.
- Modular power plants (would require an expanded supply of helium-3).
- Power plants in 3rd-world nations.

In the long term, after demonstrating the reliability, safety, and robustness of the PFRC in space or military units, we would develop a commercial reactor design. We have used established methods to estimate the future levelized cost of electricity (LCOE) of a commercial plant. This requires addressing the cost and availability of helium-3. Currently, helium-3 is obtained from the decay of tritium from nuclear weapons maintenance and CANDU fission reactors. Helium-3 may in the future be commercially produced via the extraction of helium from natural gas, or sourced from breeder fusion reactors [49, 50] or lunar or planetary mining. [51] Costs can be estimated from today's market or an assumed cost of the breeder reactor or planetary mining system.

The LCOE metric encompasses capital costs, operations and maintenance costs, performances, and fuel costs. A simple model for LCOE described by the National Renewable Energy Laboratory [52] is:

$$LCOE = \frac{OCC * CRF + O\&M_{fixed}}{8760 * CF} + C_{fuel} * Q + O\&M_{variable} \quad (5)$$

where CRF is capital recovery factor, CF is capacity factor, O&M is operations and maintenance, 8760 is the hours in a year, C_{fuel} is the fuel cost, and Q is the heat rate. The capacity factor ranges from 0 to 1 and is the portion of a year that the power plant is generating power; for fusion, this should be around 90%. Fixed O&M costs include the staff, which can be substantial for nuclear systems and are driven by regulations. The heating rate captures the total conversion efficiency from thermal output to new electricity.

We assume a terrestrial spot price of ^{3}He of $2000 per liter, or $15M per kg, while deuterium is about $14,000 per kg. A D-D breeder reactor system would consume 5 deuterium for every helium-3, which reduces the fuel cost by a factor of over 300 compared to the terrestrial helium-3, but has higher investment costs (OCC and fixed O&M for the additional reactors). Planetary mining may reduce the fuel cost by 1/15 compared to the spot price, where all the mining investment is assumed to be absorbed in the price.

With appropriate regulatory changes to reduce staff compared to fission plants, and therefore operations and maintenance costs, we estimate modular plants using 10 MW PFRC units might achieve a LCOE of $0.15/kWh with planetary helium-3, half the current cost of electricity in California, and $0.22/kWh with bred helium-3.

Summary and Next Steps

PFRC has the potential to produce a new class of modular fusion power reactors for a wide variety of applications. Results with PFRC-1 and PFRC-2 show great promise. The next machine, PFRC-3, will be needed to deepen understanding of the plasma physics of the device at fusion-relevant plasma temperatures, magnetic fields, and plasma pressures, and to test technical methods. Such considerations include efficient RMF coupling to the plasma, particle and energy transport, and energy extraction. Widespread use of PFRC will require new sources of helium-3 which may be from natural gas extraction, CANDU fission reactors, helium-3 breeding, or lunar mining.

We continue to support the PFRC-2 experiment, which is being upgraded to operate in a predicted ion heating regime at 2 MHz RMF frequency and up to 200 kW input RF power. Our team recently completed an ARPA-E OPEN award and was selected for three INFUSE awards in the first 2022 cycle. These will support computational analyses of different RF antenna configurations and FRC stability, and measurements of electron temperature profiles.

Acknowledgements This work was supported in part by ARPA-E grant DE-AR0001099, a NASA Innovative Advanced Concepts (NIAC) Grant NNX16AK28G and NASA STTRs NNX17CM47P and NNX17CC74P.

Author Contributions The authors contributed equally to this work.

Funding Advanced Research Projects Agency - Energy (ARPA-E), DE-AR0001099.

Availability of data and materials Datasets used in this paper can be accessed by request to the authors.

Declarations

Conflict of interests No competing interests.

Ethical Approval Not applicable.

References

1. S.A.Cohen, M.Chu-Cheong, R.Feder, K.Griffin, M.Khodak, J.Klabacha, E.Meier, S.Newbury, M.Paluszek, T.Rognlien, S.Thomas, M.Walsh. Reducing neutron emission from small fusion rocket engines. In: IAC (2015). IAC-15,C4.7-C3.5,9,x28852
2. E.S. Evans, S.A. Cohen, D.R. Welch, Particle-in-cell studies of fast-ion slowing-down rates in cool tenuous magnetized plasma. Phys. Plasmas **10**(1063/1), 5022188 (2018)
3. S.A. Cohen, C. Swanson, N. McGreivy, A. Raja, E. Evans, P. Jandovitz, M. Khodak, G. Pajer, T.D. Rognlien, S. Thomas, M. Paluszek, Direct fusion drive for interstellar exploration. J. Br. Interplanet. Soc. **72**(2), 38–50 (2019)

4. S.J.Thomas, M.Paluszek, S.Cohen, N.McGreivy, E.Evans. Fusion-Enabled Pluto Orbiter and Lander. In: Proceedings of the AIAA Space Forum (2017). https://doi.org/10.2514/6.2017-5276
5. Y.S. Razin, G. Pajer, M. Breton, E. Ham, J. Mueller, M. Paluszek, A.H. Glasser, S.A. Cohen, A direct fusion drive for rocket propulsion. Acta Astronautica **105**(1), 145–155 (2014). https://doi.org/10.1016/j.actaastro.2014.08.008
6. J.Mueller, A.Knutson, M.Paluszek, G.Pajer, S.Cohen, A.H.Glasser, Direct Fusion Drive Rocket for Asteroid Deflection. In: 33rd IEPC (2013). IEPC-2013-296. http://www.iepc2013.org/get?id=296
7. I.R. Jones, A review of rotating magnetic field current drive and the operation of the rotamak as a field-reversed configuration (Rotamak-FRC) and a spherical tokamak (Rotamak-ST). Phys. Plasmas **6**, 1950 (1999). https://doi.org/10.1063/1.873452
8. A.L. Hoffman, H.Y. Guo, J.T. Slough, S.J. Tobin, L.S. Schrank, W.A. Reass, G.A. Wurden, The TCS rotating magnetic field FRC current-drive experiment. Fusion Sci. Technol. **41**(2), 92–106 (2002). https://doi.org/10.13182/FST02-A205
9. R.D. Milroy, C.C. Kim, C.R. Sovinec, Extended magnetohydrodynamic simulations of field reversed configuration formation and sustainment with rotating magnetic field current drive. Phys. Plasmas **17**(6), 062502 (2010). https://doi.org/10.1063/1.3436630
10. S.A. Cohen, R.D. Milroy, Maintaining the closed magnetic-field-line topology of a field-reversed configuration with the addition of static transverse magnetic fields. Phys. Plasmas. **10**(1063/1), 874094 (2000)
11. S.A. Cohen, A.H. Glasser, Ion heating in the field-reversed configuration by rotating magnetic fields near the ion-cyclotron resonance. Phys Rev Lett (2000). https://doi.org/10.1103/PhysRevLett.85.5114
12. T. Ahsan, S.A. Cohen, An analytical approach to evaluating magnetic-field closure and topological changes in FRC devices. Phys Plasmas **29**(7), 072507 (2022). https://doi.org/10.1063/5.0090163
13. D. Welch, S.A. Cohen, T.C. Genoni, A.H. Glasser, Formation of field-reversed-configuration plasmas with punctuated-betatron-orbit electrons. Phys. Rev. Lett. **105**, 015002 (2010). https://doi.org/10.1103/PhysRevLett.105.015002
14. A.H. Glasser, S.A. Cohen, Ion and electron acceleration in the field-reversed configuration with an odd-parity rotating magnetic field. Phys Plasmas. **10**(1063/1), 1459456 (2002)
15. S.A. Cohen, A.S. Landsman, A.H. Glasser, Stochastic ion heating in a field-reversed configuration geometry by rotating magnetic fields. Phys Plasmas **14**, 072508 (2007). https://doi.org/10.1063/1.2746813
16. A.H. Glasser, S.A. Cohen, Simulating single-particle dynamics in magnetized plasmas: The RMF code. Rev. Sci. Instrum. **93**, 083506 (2022). https://doi.org/10.1063/5.0101665
17. S.A. Cohen, B. Berlinger, C. Brunkhorst, A. Brooks, N. Ferarro, D. Lundberg, A. Roach, A.H. Glasser, Formation of collisionless high-β plasmas by odd-parity rotating magnetic fields. Phys. Rev. Lett **98**, 145002 (2007). https://doi.org/10.1103/PhysRevLett.98.145002
18. O. Seeman, I. Be'ery, A. Fisher, Stabilization of magnetic mirror machine using rotating magnetic field. J. Plasma Phys. (2018). https://doi.org/10.1017/S0022377818000971
19. S.Cohen, C.Brunkhorst, A.Glasser, A.Landsman, D.Welch, RF plasma heating in the PFRC-2 device: Motivation, goals and methods. In: AIP Conference Proceedings, vol. 1406 (2011). https://doi.org/10.1063/1.3664976
20. C.E. Myers, M.R. Edwards, B. Berlinger, A. Brooks, S.A. Cohen, Passive superconducting flux conservers for rotating-magnetic-field-driven field-reversed configurations. Fusion Sci. Technol. **61**(1), 86–103 (2012). https://doi.org/10.13182/FST12-A13341
21. B. Berlinger, A. Brooks, H. Feder, J. Gumbas, T. Franckowiak, S.A. Cohen, Use of polycarbonate vacuum vessels in high-temperature fusion-plasma research. Fusion Sci. Technol. **64**(2), 298–302 (2013). https://doi.org/10.13182/FST13-A18093
22. S.A.Cohen, D.Stotler, M.Buttolph, Fueling Method for Small, Steady-State, Aneutronic FRC Fusion Reactors. U.S. Patent 10,811,159 (2020)
23. M.A.Paluszek, E.M.Ham, Y.Razin, S.A.Cohen, In space startup method for nuclear fusion rocket engines. U.S. Patent 10,229,756 (2019)
24. M.A.Paluszek, S.J.Thomas, S.A.Cohen, Space nuclear power systems - direct fusion drive. In: 2018 International Energy Conversion Engineering Conference (2018). https://doi.org/10.2514/6.2018-4974
25. H. Momota, A. Ishida, Y. Kohzaki, G.H. Miley, S. Ohi, M. Ohnishi, K. Sato, L.C. Steinhauer, Y. Tomita, M. Tuszewski, Conceptual design of the D-^{3}He reactor artemis. Fusion Technol. **21**, 2307 (1992). https://doi.org/10.13182/FST92-A29724
26. R. Chapman, G.H. Miley, W. Kernbichler, M. Heindler, Fusion space propulsion with a field reversed configuration. Fusion Technol. **15**,1154 (1989). https://doi.org/10.13182/FST89-A39849
27. H. Nakashima, G.H. Miley, Y. Nakao, Field reversed configuration (FRC) fusion rocket. AIP Conf Proceed. **301**, 1311 (1994). https://doi.org/10.1063/1.2950141
28. V.I. Khvesyuk, S.V. Ryzhkov, J.F. Santarius, G.A. Emmert, C.N. Nguyen, L.C. Steinhauer, D-^{3}He field reversed configuration fusion power plant. Fusion Technol. **39**, 410 (2001). https://doi.org/10.13182/FST01-A11963492
29. S.Thomas, C.Swanson, M.Paluszek, S.Cohen, S.Turyshev, Fusion propulsion and power for extrasolar exploration. In: IAF Space Propulsion Symposium, International Astronautical Congress (2019)
30. M. Tuszewski, Field reversed configuration confinement enhancement through edge biasing and neutral beam injection. Phys Rev Lett **108**, 255008 (2012). https://doi.org/10.1103/PhysRevLett.108.255008
31. M.W. Binderbauer, T. Tajima, L.C. Steinhauer et al., A high performance field-reversed configuration. Phys Plasmas **22**(5), 056110 (2015). https://doi.org/10.1063/1.4920950
32. E.A. Baltz, E. Trask, M. Binderbauer, M. Dikovsky, H. Gota, R. Mendoza, J.C. Platt, P.F. Riley, Achievement of Sustained Net Plasma Heating in a Fusion Experiment with the Optometrist Algorithm. Sci Rep **7**, 6425 (2017). https://doi.org/10.1038/s41598-017-06645-7
33. H. Gota, M.W. Binderbauer, T. Tajima et al., Overview of C-2W: high temperature, steady-state beam-driven field-reversed configuration plasmas. Nuclear Fusion **61**(106039), (2021). https://doi.org/10.1088/1741-4326/ac2521
34. K.Nguyen, T.Kammash, :Classical Transport Coefficients in A Field-Reversed Configuration. Plasma Physics **24**(2) (1982)
35. A. Ishida, H. Momota, L.C. Steinhauer, Variational formulation for a multifluid flowing plasma with application to the internal tilt mode of a field-reversed configuration. Phys Fluids **31**(10), 3024–3034 (1988). https://doi.org/10.1063/1.866959
36. J.Lyman Spitzer, Physics of Fully Ionized Gases, 2nd edn., p. 145 (1962)
37. C.Swanson, P.Jandovitz, S.A.Cohen, Using Poisson-regularized inversion of Bremsstrahlung emission to extract full electron energy distribution functions from x-ray pulse-height detector data. In: AIP Advances, vol. 8, p. 025222 (2018). https://doi.org/10.1063/1.5019572
38. C.Biava, G.Wilkie, A.Dogariu, S.Cohen, Modeling spatially resolved neutral atom densities in the PFRC-2 using DEGAS 2.

In: 63rd Annual Meeting of the APS Division of Plasma Physics (2021)
39. C.A. Galea, C.P.S. Swanson, S.A. Cohen, S.J. Thomas, Use of a Mylar filter to eliminate vacuum ultraviolet pulse pileup in low-energy x-ray measurements. Rev. Sci. Instrum. **93**(9), 093531 (2022). https://doi.org/10.1063/5.0101712
40. M. Notis, A.Glasser, S.Cohen, S.Abe, Electrostatic Energy Analyzer and Gas Stripping Cell to Measure Ion Temperature in the PFRC-2. In: APS Division of Plasma Physics Meeting Abstracts. APS Meeting Abstracts, vol. 2021, pp. 11–192 (2021). https://ui.adsabs.harvard.edu/abs/2021APS..DPPJP1192N
41. J.A.Sims, Jupiter Icy Moons Orbiter Mission Design Overview. In: AAS/AIAA Space Flight Mechanics Conference, Tampa, Florida (2006)
42. J.Staff, Prometheus project final report. Technical Report 982-R120461, Jet Propulsion Laboratory (October 2005)
43. J. Gould, *All-electric brigades?* (US Army official says it's coming sooner than you'd think, Defense News, 2017)
44. J.Trevithick, The Army Wants Its Brigades To Be Able To Fight For An Entire Week Without Resupply. The War Zone (2018)
45. S.J.Matthews, Small Tactical Electric Power. CERDEC CPI Power Division (2015). https://arpa-e.energy.gov/sites/default/files/Matthew_CERDEC_GENSETS_FINAL.pdf Accessed 08-18-2022
46. J.Keller, Navy to test large unmanned submarine next year in open-ocean voyage down the california coast. Military + Aerospace Electronics (2015). Accessed 2022-08-18
47. M.L.Jones, Remote-Site Power Generation Opportunities for Alaska, Topical Report. Technical Report DE-FC21-93MC30098, Energy and Environmental Research Center (March 1997)
48. Hatch: SMR Deployment Feasibility Study: Feasibility of the Potential Deployment of Small Modular Reactors (SMRs) in Ontario. Technical Report H350381-00000-162-066-0001, Rev. 0, Ontario Ministry of Energy (June 2016)
49. V.I. Khvesyuk, A.Y. Chirkov, Low-radioactivity D-^{3}He fusion fuel cycles with ^{3}He production. Plasma Phys Controll Fusion (2002). https://doi.org/10.1088/0741-3335/44/2/308
50. J. Kesner, DT, Garnier,A.Hansen, M.Mauel, L.Bromberg, Helium catalyzed D-D fusion in a levitated dipole. Nuclear Fusion 44, 193 (2004)
51. L.J.Wittenberg, J.F.Santarius, G.L.Kulcinski. Lunar Sources of ^{3}He for commercial fusion power. Fusion Technol. 10, 167 (1986). https://doi.org/10.13182/FST86-A24972
52. NREL.gov: Simple levelized cost of energy (LCOE) calculator documentation. Accessed 2022-08-19